The Energy Dependence of the Resonant Scattering of Slow Neutrons from Gold*

JAY TITTMAN AND CHARLES SHEER
Department of Physics, Columbia University, New York, New York

(Received January 31, 1951)

The energy dependence of slow neutrons scattered from a thick gold target has been measured using a newly developed scattering chamber in conjunction with the Columbia slow neutron velocity spectrometer. A method of analysis has been developed for determining the ratio of the scattering cross section to the total cross section, σ_s/σ_t, as a function of energy for an "unknown" sample in terms of a calibration target for which $(\sigma_s/\sigma_t)(E)$ is known.

The agreement between the experimental determination of $(\sigma_s/\sigma_t)(E)$ for gold in the energy range 0.7 to 8 ev and the Breit-Wigner theory is excellent. All the level parameters can be evaluated by combining these scattering data with the results of transmission experiments and the cross section for self-indication. The final results for the 4.9-ev gold level are: $J=1$, $\Gamma=0.172$ ev, $\Gamma_N=0.0211$ ev, $R_{J=1}=1.03$ barn$^{\frac{1}{2}}$, $R_{J=2}=0.917$ barn$^{\frac{1}{2}}$.

I. INTRODUCTION

THE Breit-Wigner equations for nuclear resonance phenomena have been derived from several different viewpoints.[1-3] However, the mechanism of excited compound nucleus formation with subsequent decay, as originally suggested by Bohr,[4] remains intact through all the derivations. For slow neutron interactions it is usually necessary to consider only elastic scattering and radiative capture. The one level expressions for these cross sections for a single isotope can be written as

$$\sigma_c(E)=\sigma_{c0}\Gamma^2(E_0/E)^{\frac{1}{2}}/[4(E-E_0)^2+\Gamma^2]$$

and

$$\sigma_s(E)=(G_\pm\sigma_{p\pm}+G_\mp\sigma_{p\mp})+4\pi G_\mp\left[\frac{\lambda_0^2\Gamma_N^2+4\lambda_0\Gamma_N R_\mp(E-E_0)}{4(E-E_0)^2+\Gamma^2}\right],$$

where σ_c = capture cross section; $\sigma_{c0}=4\pi\lambda_0^2 G_\mp\Gamma_N\Gamma_\gamma/\Gamma^2$ = capture cross section at the energy of exact resonance, E_0; $\Gamma=\Gamma_N+\Gamma_\gamma$ = total level width; Γ_N = neutron width at exact resonance; Γ_γ = gamma-ray width; σ_s = scattering cross section; $\lambda_0=(\frac{1}{2}\pi)\times$neutron wavelength at the resonance energy, E_0; $G=(2J+1)/[(2I+1)(2S+1)]$ = statistical weight; R = effective nuclear radius; σ_p = potential scattering cross section $(=4\pi R^2)$. The statistical weight factor G, where $J=I\pm S$, depends upon the relative orientation of the spins of the incident neutron and of the struck nucleus. The subscripts $\pm$ and $\mp$ are included to designate quantities which depend specifically on the total spin quantum number of the system, J, for the collision. For example $(G_\pm\sigma_{p\pm})$ is the contribution to the total potential scattering cross section from collisions which do not satisfy the necessary spin condition for resonance (in the case of a mono-isotopic material). Here $(G_\mp\sigma_{p\mp})$ is the contribution from collisions which do have the appropriate total spin. Thus, the total potential scattering cross section σ_p is

$$\sigma_p=G_\pm\sigma_{p\pm}+G_\mp\sigma_{p\mp}=4\pi R_{\text{eff}}^2,$$

where R_{eff} is the effective nuclear radius for the isotope involved and is not necessarily the same as $R_\mp$, which is the effective nuclear radius for collisions which have total spin equal to the J of the level at E_0.

The capture cross section has the straightforward damped resonance form, modulated by the $1/v$ factor. Here σ_s shows the addition of potential and resonance scattering and also contains a term arising from the interference[5] between these two effects. This interference results in a depression of σ_s on the low energy side of resonance and an augmentation on the high energy side. It is worthy of note that at the minimum of the depression, $\sigma_s=G_\pm\sigma_{p\pm}$.

Although an abundance of data has been collected on epithermal cross sections for the elements,[6-14] detailed measurements of σ_s as a function of energy have been restricted to regions in which the capture process plays

* For preliminary reports see Tittman, Sheer, Rainwater, and Havens, Phys. Rev. **77**, 748(A) (1950); **80**, 903 (1950); **82**, 344 (1951).

[1] G. Breit and E. Wigner, Phys. Rev. **49**, 519 (1936); H. A. Bethe and G. Placzek, Phys. Rev. **51**, 450 (1937); Kalckar, Oppenheimer, and Serber, Phys. Rev. **52**, 273 (1937); Kapur and R. E. Peierls, Proc. Roy. Soc. (London) **A166**, 277 (1938); Arnold J. F. Siegert, Phys. Rev. **56**, 750 (1939); G. Breit, Phys. Rev. **69**, 472 (1946); E. Wigner, Phys. Rev. **70**, 15, 606 (1946); E. P. Wigner and L. Eisenbud, Phys. Rev. **72**, 29 (1947).

[2] H. A. Bethe, Revs. Modern Phys. **9**, 69 (1937).

[3] Feshbach, Peaslee, and Weisskopf, Phys. Rev. **71**, 145, 564 (1947).

[4] N. Bohr, Nature **137**, 344 (1936).

[5] For curves illustrating this effect in In see reference 3.

[6] Goldsmith, Ibser, and Feld, Revs. Modern Phys. **19**, 259 (1947).

[7] L. J. Rainwater and W. W. Havens, Phys. Rev. **70**, 136 (1946).

[8] W. W. Havens and L. J. Rainwater, Phys. Rev. **70**, 154 (1946).

[9] Rainwater, Havens, Wu, and Dunning, Phys. Rev. **71**, 65 (1947).

[10] Havens, Wu, Rainwater, and Meaker, Phys. Rev. **71**, 165 (1947).

[11] Wu, Rainwater, and Havens, Phys. Rev. **71**, 174 (1947).

[12] Rainwater, Havens, Dunning, and Wu, Phys. Rev. **73**, 733 (1948).

[13] Havens, Rainwater, Wu, and Dunning, Phys. Rev. **73**, 963 (1948).

[14] References 6 through 13 contain additional bibliographies.

a negligible role. At these higher energies the potential-resonance interference has been observed in the case of S-wave scattering from sulfur.[15] At lower energies the Cd resonance has been investigated in detail by transmission measurements.[7,9] However, the only information on scattering in the low energy resonance region has been obtained through the use of resonance scattering detectors or other methods involving the determination of level parameters by means of the measurement of integrals of $\sigma_s(E)$ and/or $\sigma_c(E)$ over relatively broad energy regions.[16–22]

The present paper describes the development of a method for the measurement of the energy dependence of neutron scattering from thick targets and the conversion of this measurement into $(\sigma_s/\sigma_t)(E)$, the ratio of the scattering cross section to the total cross section. Of course, measurements of this type will be of value only in cases where some capture is present. The method consists essentially of the use of the Columbia slow neutron velocity spectrometer[7,9] (NVS) for the energy sorting of neutrons scattered by a thick target. The counting rates are then compared with those due to standard targets of known σ_s/σ_t. Gold has been chosen as the first element to be studied for a number of reasons. It possesses a strong, isolated resonance in an energy region in which the cyclotron intensity is sufficiently high to enable the use of good resolution with the NVS.[8,10] It is a mono-isotopic element of small spin ($I=\frac{3}{2}$) so that the effect of whether $J=I+\frac{1}{2}$ or $I-\frac{1}{2}$ is relatively large. Furthermore, Au has been used in several other experiments as a standard,[22,23] using approximate values for the level parameters, and it was thought desirable to determine these parameters with greater precision than has been done heretofore.

The measurement of $(\sigma_s/\sigma_t)(E)$ does not uniquely determine all the level parameters. However, as will be indicated later, other techniques can be used to fix the remaining unknown ones.

In the remainder of this paper the subscripts t, s, and c refer to total, scattering, and capture, respectively. The subscript 0 refers to a value at exact resonance; for example, $(\sigma_{t0})_{Au}$ is the total cross section for Au at exact resonance. All cross sections are expressed in barns, b (1 b$=10^{-24}$ cm^2).

II. APPARATUS DESCRIPTION

The Columbia NVS has already been described in detail.[7,9] The present application differs essentially from former ones in that the path of flight of the neutrons now consists of the distance from the paraffin source slab, near the Be cyclotron target, to the scattering target, plus the distance from the scattering target to the BF_3 counter banks. The scattering chamber, a horizontal section of which is illustrated in Fig. 1, is placed in position relative to the cyclotron in a manner similar to that used in the collimating system shown in Fig. 2, reference 7. The neutron beam passes through a hole in the water tanks forming the cyclotron enclosure, is collimated, and strikes the thick scatterer; and the scattered neutrons are detected by the BF_3 proportional counters.

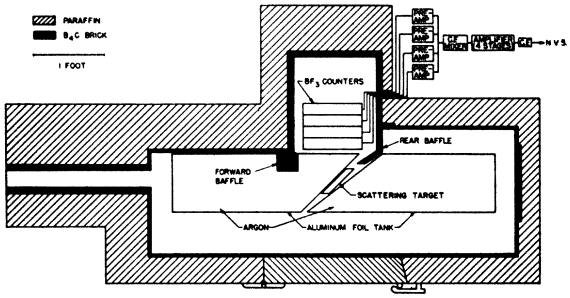

FIG. 1. Schematic drawing of a horizontal section of the neutron scattering chamber.

The inside walls of the scattering chamber are completely lined with B_4C bricks to reduce as much as possible the scattering of neutrons from the walls into the counters. At least 3 inches of paraffin surrounds the B_4C liner to prevent stray fast neutrons outside the cyclotron enclosure from entering the chamber.

The collimator is 3 inches square in cross section, also lined with B_4C bricks to decrease as much as possible "inscattering" to the target and the counters. The principle of design, insofar as the collimator and forward baffle are concerned, requires that no line of sight exist from any point on the collimator wall lining, exposed to the main neutron flux, to the counters. This prevents even the relatively small number of neutrons singly scattered from the collimator walls from contributing to the background. The forward baffle allows the counter banks to be moved close to the scattering target, thus subtending from it a large solid angle, without exposing them to an increased background. By using a thin aluminum target holder, very little extraneous material is exposed to the direct neutron beam to contribute unwanted scattered neutrons to the counting rate to be measured.

The B_4C bricks on the rear wall of the chamber serve as a sink for those neutrons which are either transmitted through the scattering target or pass by its sides. Since even B_4C, however, is not a perfect neutron sink material, some neutrons are backscattered from the backstop, particularly at high energies. Although many of these are captured by the thick scattering target on their way to the counters, some could pass between the

[15] Adair, Bockelman, and Peterson, Phys. Rev. **76**, 308 (1949); Peterson, Barschall, and Bockelman, Phys. Rev. **79**, 593 (1950).
[16] Harris, Seidl, and Langsdorf, Phys. Rev. **72**, 866 (1947).
[17] F. G. P. Seidl, Phys. Rev. **75**, 1508 (1949).
[18] C. T. Hibdon and C. O. Muehlhause, Phys. Rev. **76**, 100 (1949).
[19] C. O. Muehlhause, Phys. Rev. **77**, 739(A) (1950).
[20] Hibdon, Muehlhause, Selove, and Woolf, Phys. Rev. **77**, 730 (1950).
[21] M. Hamermesh and C. O. Muehlhause, Phys. Rev. **78**, 175 (1950).
[22] Harris, Muehlhause, and Thomas, Phys. Rev. **79**, 11 (1950).
[23] H. Pomerance, Phys. Rev. **77**, 747(A) (1950).

scatterer and the upper wall of Fig. 1. To intercept the latter, the rear baffle has been inserted. This baffle extends out into the chamber sufficiently far to intercept most of the backscattered neutrons which would have contributed to background, but not so far as to project into the primary beam.

As a result of these measures in regard to materials and geometry, most of the remaining background would be due to those neutrons multiply scattered from the walls of the chamber and those scattered by air along the path of the incident beam. The air scattering has been eliminated to a large extent by utilizing the very small scattering cross section (0.68 b) of argon.[24] Since it is not feasible to evacuate the chamber, most of the air path has been replaced by an argon path at atmospheric pressure. The argon is contained in the aluminum tanks, shown schematically in Fig. 1. The sides of the tanks are made of 0.004-inch aluminum foil, and the front and back ends, through which the beam passes, are of 0.002-inch foil. Despite the air space remaining between the two tanks and the two aluminum walls before and after the target, it was found that the use of argon to replace air effected an improvement of a factor of two in reduction of background.

The BF_3 proportional counters are stacked in four vertical banks of five counters each, and supported by a thin aluminum framework. The counters all have essentially the same characteristics insofar as pulse height and plateau region are concerned.[25] The outputs of the five counters in each bank are connected in parallel, each bank feeding into its own low input impedance preamplifier. The four preamplifiers then feed their output pulses in parallel onto the grid of a cathode follower and thence to a conventional pulse amplifier (Fig. 1). The pulse amplifier sends approximately 5-volt output pulses to the NVS. Each counter output passes through a plug panel before entering the parallel feed connection into the preamplifier for the bank in which the counter rests. This allows the output of each counter individually to be viewed on an oscilloscope for test purposes. The negative high voltage for the counters, supplied by a radiofrequency high voltage supply, is applied to all the counters in parallel. The $\frac{1}{32}$-inch brass counter cathodes and aluminum frame are contiguous so that the whole assembly is at negative high voltage. The frame stands on 1-inch quartz legs. The gains of the preamplifiers are equalized so that the output pulse height is independent of the counter bank in which the pulse originates. The amplifier output pulses fed to the NVS have a rise time of approximately 0.1 microsecond and width at half-maximum of less than 1 microsecond. The counter voltage, amplifier gain, and NVS level setter are adjusted to give as large a counting rate as possible consistent with the condition that no γ-rays be counted, as determined by tests using strong γ-ray sources.

The time of flight resolution of this system is slightly broadened over that which is encountered in the case of transmission experiments using the NVS. Principally, this is due to the relatively large size (4×6 inches) of the scattering target, depth (8 inches) of the detection volume, and large (~15 percent of total) solid angle subtended by the counters at the target. However, as will be shown later, high resolution is not necessary for the present scattering measurements, and in all cases resolution effects were negligible.

Since the various neutron rays traverse slightly different distances before being counted, it is difficult to assign a measured path length to the path of flight. To fix this value, however, since it is necessary for the determination of the velocity of the scattered neutrons, the following procedure was used. With a thick carbon scatterer in position, to provide high counting rates, the system was used as a scattering detector of slow neutrons, and transmission measurements *vs* time of flight were made for thin Au, In, and Co filters placed before the collimator. Since all of these materials have sharp resonances at well-determined neutron energies, it is possible to determine[7] the effective over-all delay time, t_d', and the effective source-detector distance d with good accuracy from the measured timings for these resonance dips. Use of the three filters mentioned above produced values of t_d' between 8.25 and 9.25 microseconds, which agree well with the independently and more directly measured value of Rainwater and Havens.[26] In this fashion, a mean value of 5.67 meters was measured for the total path of flight.

The background counting rate was about 2 percent of the counting rate due to scattering from a thick carbon target between about 1 and 100 ev.

A test to determine the geometrical width of the beam at the position of the scatterer was made by comparing the scattered neutron counting rates from carbon scatterers of the same thickness and varying widths. This test showed the beam intensity to be constant out to 1.5 inches from the beam axis, dropping to 50 percent of maximum at 2.0 inches, and to 1 percent at 3.5 inches. Thus, the target size was chosen to be 4 inches ×6 inches. Since the target is at 45° to the neutron beam, approximately a projected 4 inch×4 inch square target faces the beam, and an equal projected area faces the counters. This geometry provided a maximum counting rate for a given scatterer, consistent with reasonable resolution.

III. EXPERIMENT ANALYSIS

For a very thin target the number of neutrons scattered should be proportional to the scattering cross section; therefore, by comparing the counting rate due to an "unknown" sample with the counting rate due to

[24] Edward Melkonian, Phys. Rev. **76**, 1750 (1949).

[25] These excellently uniform counters were obtained from the Oak Ridge National Laboratory.

[26] L. J. Rainwater and W. W. Havens, Jr., private communication.

a thin standard such as carbon, the value of $\sigma_s(E)$ could be obtained. Because in many cases this requires inordinately small geometric target thickness and results in extremely low counting rates, a thick target approach has been used for the present measurements. Furthermore, the thin target technique would require far greater cyclotron intensity than is now available for the investigation of resonances, as complete resolution of the level would be necessary unless an integration method of analysis were used.

In order to analyze the significance of the number of scattered neutrons counted with an infinitely thick scatterer, assume the target nucleus to be infinitely heavy so that the neutron suffers no energy loss in the collision. Since only neutron energies well above the thermal region are considered and the solid angle subtended by the detector is fairly large, only free cross sections need be considered. We temporarily neglect the background counting rate. Then, using Fig. 2, which indicates the geometry of the scattering, it can be shown by the method outlined in Appendix A, that the ratio of the counting rate due to neutrons scattered from an *infinitely thick* target of material x to that from a thick carbon target C, is

$$N_x/N_C=\sum_{j=1}^{\infty} g_j(\sigma_s/\sigma_t)^j{}_x\equiv F(\sigma_s/\sigma_t)_x, \qquad (1)$$

where g_j are coefficients depending only on the geometry of the experiment, and j represents the multiplicity of the scattering; i e., the jth term represents the contribution to the counting rate made by neutrons scattered j times. Note that in Eq. (1) the energy dependence of the ratio N_x/N_C arises solely through the quantity σ_s/σ_t.

The criterion that a target be thick enough to use the "infinite thickness" approximation depends upon the value of σ_s/σ_t. If $(\sigma_s/\sigma_t)<\sim 0.5$, for our geometry, the requirement that the transmission, T, be less than 0.1 is satisfactory to within about 1 percent (see Appendix A). If $(\sigma_s/\sigma_t)>\sim 0.5$, so that more than the first few terms in Eq. (1) contribute appreciably to the scattered neutron counting rate, the appropriate criterion for thickness is that the ratio of geometrical target slant thickness, a, to diffusion length shall be large. All the scatterers used in the present measurements had $T<0.1$ over the range of energy in which they were used. Hence, the results are accurate for measured values of $(\sigma_s/\sigma_t)<\sim 0.5$.

The theoretical evaluation of the g_j with any degree of accuracy for the present "poor geometry" experiment (see Figs. 1 and 2) is extremely difficult. However, by using a standard calibration scatterer, x_0, and measuring $F(\sigma_s/\sigma_t)_{x_0}$, the apparatus can be calibrated experimentally. Subsequent measurement of $F(\sigma_s/\sigma_t)_x$, as a function of E, where x represents the "unknown" scatterer, and comparison with the calibration curve, then yields $(\sigma_s/\sigma_t)_x(E)$. As long as the standard target

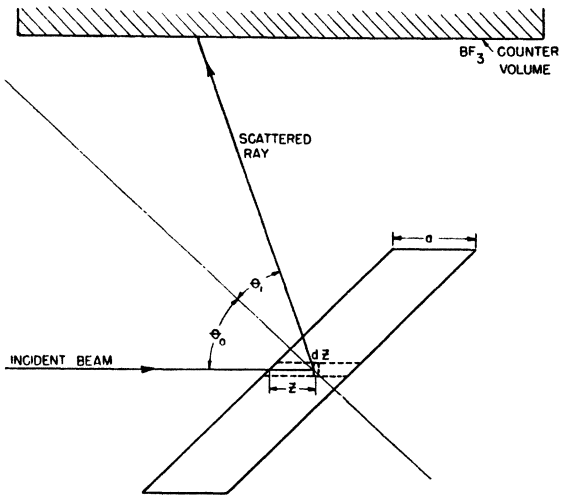

FIG. 2. Horizontal section of target and counters showing the geometry for single scattering analysis.

x_0 and the target x have nearly the same geometrical thickness and not too low atomic weight, the geometry of scattering is essentially the same for both. Therefore, the edge effects occurring for x are nearly identical with those occurring for x_0, and, since both effects are small, the difference between them has been neglected within the accuracy of the present measurements.

The standard targets, x_0's, used were Ni_2B and B_2O_3. By using two standard targets having widely different atomic weights, and overlapping ranges of σ_s/σ_t, two independent determinations of the calibration function were made. Since these were mutually consistent, Eq. (1) was verified. The choice of these compounds for standards was based upon the appropriateness of the range of variation of their σ_s/σ_t values in setting up the calibration function for the apparatus.

IV. APPROXIMATIONS AND CORRECTIONS

The neglect of background counting rate and neutron energy loss on collision (finite nuclear mass effect) necessitates correction of the scattering data.

Since all the scatterers used had very small transmission, the background depended upon whether or not a target was in position. The ideal method of background determination would have been the replacement of the scattering target by a target of infinite thickness and zero scattering cross section. This target would then have contributed no scattered neutrons to the background counting rate and at the same time would have carried out the absorbing function because of its infinite thickness. For this purpose a target of B^{10} was used. Although B^{10} does not have $\sigma_s=0$, it does have $(\sigma_s/\sigma_t)\ll 1$.[27] The method of correcting for the B^{10} scattering contribution to the background is discussed in Appendix B.

The assumption that the struck nucleus is of infinite

[27] The relevant properties of B^{10} are given in Sec. VII.

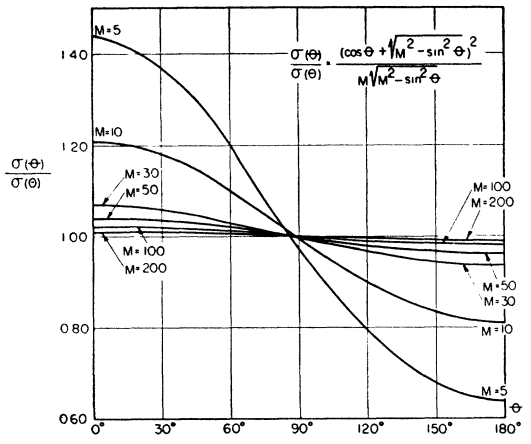

FIG. 3. Ratio of differential scattering cross sections in the laboratory and center-of-mass systems as a function of laboratory scattering angle, varying the parameter M.

mass, used in arriving at Eq. (1), is obviously not exactly satisfied by any of the targets used in this experiment. The corrections which must be considered because of this occur in the conversion of the center-of-mass system of coordinates into the laboratory system. In nearly all cases they are quite small. The following effects are taken into account:

A. Asymmetry of the angular distribution of scattered neutrons in the laboratory system.

B. Dependence of counter sensitivity on the neutron energy after collision rather than on the energy before the collision.

C. Difference between total cross section of the target before and after collision, resulting from the change in energy of the neutron during collision and the energy dependence of the σ_t of the target material.

The corrections for these effects have been applied considering only singly scattered neutrons.

A. Since only S-wave scattering occurs at low energies, $\sigma_s(\Theta)$, the differential scattering cross section in center-of-mass coordinates is spherically symmetric. Thus, the angular dependence of scattering, in the laboratory system, is determined by[28]

$$\frac{\sigma_s(\theta)}{\sigma_s(\Theta)}=\frac{[\cos\theta+(M^2-\sin^2\theta)^{\frac{1}{2}}]^2}{[M(M^2-\sin^2\theta)^{\frac{1}{2}}]}, \tag{2}$$

where θ is the scattering angle in the laboratory system, and M is the ratio of the mass of the struck nucleus to the mass of the incident particle. In the present case the latter is merely the atomic weight of the scattering nucleus. A plot of Eq. (2) is shown in Fig. 3 for various M. Reference to the geometry of Figs. 1 and 2 indicates that the probability of counting a scattered neutron is, on the average, approximately symmetrical about the scattering angle $\theta=90°$. From the form of $\sigma_s(\theta)/\sigma_s(\Theta)$ the deficiency of scattered neutrons in the backward direction is approximately compensated by the excess in the forward direction. Even for moderately low M the unbalance about 90° is small, and for the larger values of M used throughout most of this experiment it is quite negligible.

B. Since the BF_3 counters used have very low detection efficiency in the energy range covered in this experiment, the detection sensitivity can be written as $S\propto 1/v'$, where v' is the neutron velocity in the counter. In the laboratory system the neutron velocity after collision, v', is related to the velocity before collision, v, by[28]

$$v'/v=[1-[2M/(M+1)^2](1-\cos\Theta)]^{\frac{1}{2}}. \tag{3}$$

Setting $\Theta=\theta$ and using $\langle\Theta\rangle_{Av}=90°$, Eq. (3) was applied as a correction factor to all measured counting rates after correction for background (see Appendix B).

C. Since the neutron loses energy on collision and σ_t of the target varies with energy, the mean free path for interaction of the neutron while directed out of the target after collision is different from that while directed into the target prior to collision. In the derivation of Eq. (1) it was assumed that these two were identical (see Appendix A). The approximate, energy dependent correction factor applied to counting rates to take cognizance of this effect is $(\sigma_t+\sigma_t')/2\sigma_t$, where σ_t is the total cross section of the target material before collision, and σ_t' is the total cross section for neutrons of energy $E'<E$ after collision (see Appendix B). With Θ again set equal to $\langle\Theta\rangle_{Av}=90°$, E' was determined from Eq. (3). For all targets which have $\sigma_t(E)$ a slowly varying function, such as Ni_2B and B_2O_3, this factor varies slowly and monotonically with E. In the vicinity of a resonance, however, as in the case of Au, it takes the shape indicated in Fig. 4. Here, even though the energy loss is only 1 percent, $(\sigma_t)_{Au}$ is varying rapidly and σ_t' is appreciably different from σ_t. Although the correction appears quite large near resonance, the smearing action of the NVS resolution

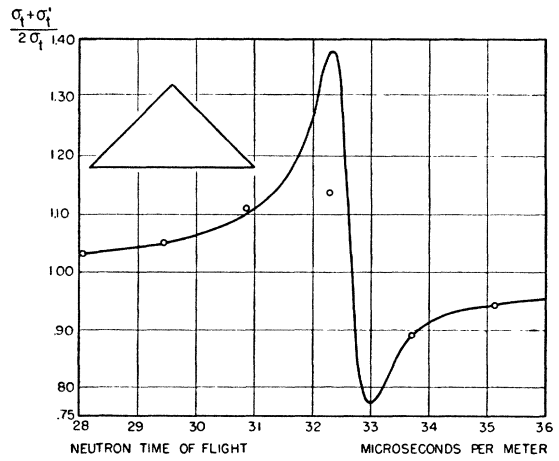

FIG. 4. The correction factor $(\sigma_t+\sigma_t')/2\sigma_t$ for Au, calculated using the parameters for $J=1$, Table II, and $E'=0.99E$. Solid curve is calculated; open circles are the actual correction factors used, determined by numerical integration of the resolution triangle over the calculated curve.

[28] See reference 2, p. 171.

reduces the effect on the counting rate. Thus, in applying the correction in the immediate vicinity of resonance, the integral of $(\sigma_t+\sigma_t')/2\sigma_t$ over the resolution function was used. The effect of this is seen in Fig. 4, where the circles indicate the correction factors actually used with the scattering data taken at the same neutron times of flight.

The net effect of the corrections discussed above, because of compensation, amounts to less than 2.2 percent in the case of B_2O_3 and to less than 0.2 percent for Ni_2B. For Au the only appreciable one is correction C, which is less than 2.5 percent over most of the energy range covered. The few points immediately near resonance have larger corrections, as indicated in Fig. 4.

From Fig. 7 it is seen that the region of principal interest is that of $(\sigma_s/\sigma_t)<\sim 0.5$. Since multiple scattering effects are of the order $(\sigma_s/\sigma_t)^i$, corrections to higher order scattering have been neglected.

It is estimated that $F(\sigma_s/\sigma_t)$, the calibration function shown in Fig. 6, is accurate to within 2 percent for $(\sigma_s/\sigma_t)<\sim 0.5$, apart from errors occurring in the values of the measured quantities used in the correction factors. Here $F(\sigma_s/\sigma_t)_{Au}$ is estimated to be accurate to within 1 percent over most of the time of flight range used in its measurement, with the exception of those points lying within about 4 microseconds/meter on either side of exact resonance; these latter are probably accurate to about 4 percent. In all cases errors due to counting statistics are larger than those discussed above; thus, errors in the level parameters come principally from this source.

V. THE SCATTERING TARGETS

All targets used in the present experiment were in the form of solid slabs or canned powders having the shape indicated in Fig. 2. Since the targets were thick, the vertical edges were cut at 45° so that all portions of the target presented the same thickness to the neutron beam. Table I indicates the pertinent properties of the targets used.

VI. SCATTERING MEASUREMENTS

The targets were inserted in the neutron beam in cyclic fashion, the number of monitor counts being adjusted to require a change of target about every half-hour. For the measurements of the calibration function $F(\sigma_s/\sigma_t)$, for example, the cycle was run as follows: Ni_2B, B_2O_3, B^{10}, C; and for the measurement of $F(\sigma_s/\sigma_t)_{Au}$: Au, Ni_2B, B^{10}, C. The purpose of cycling the targets is to average out slow drifts in counter voltage, amplier gain, level set height, and cyclotron monitor detection efficiency.

X-ray analysis of the Ni_2B target[29] indicated strong Bragg reflection planes with spacings of from 0.775A to 0.923A. Since first- and second-order scattering from these planes, for the geometry used, would affect the calibration curve, the only scattering data used were taken at neutron energies >1 ev.

The excellent agreement between the two sets of data (Ni_2B and B_2O_3) for measurements taken at $E>1$ ev substantiates the corrections made. The three lowest points in Fig. 6 were taken between 0.2 and 1 ev using the B_2O_3 scatterer which has, unlike Ni_2B, a vitreous structure.

VII. TRANSMISSION MEASUREMENTS[7,8]

The $1/v$ regions of the B^{10}, Ni_2B, and B_2O_3 cross sections were investigated using the apparatus and methods previously described[7–13] in order to determine their σ_s/σ_t values. Least-squares fits to the measured transmissions yielded for these samples

$$(\sigma_t)_{B_{10}}=(0.94\pm 1)+(646\pm 22)E^{-\frac{1}{2}}\text{ b},$$
$$(\sigma_t)_{Ni_2B}=(40.2\pm 1)+(133\pm 3)E^{-\frac{1}{2}}\text{ b},$$
$$(\sigma_t)_{B_2O_3}=(20.9\pm 1.5)+(218\pm 3.5)E^{-\frac{1}{2}}\text{ b}.$$

Using the constant terms as the respective σ_s, these become

$$(\sigma_s/\sigma_t)_{B_{10}}=(1+690E^{-\frac{1}{2}})^{-1},$$
$$(\sigma_s/\sigma_t)_{Ni_2B}=(1+3.31E^{-\frac{1}{2}})^{-1},$$
$$(\sigma_s/\sigma_t)_{B_2O_3}=(1+10.4E^{-\frac{1}{2}})^{-1}.$$

These were the values used in the determination of $F(\sigma_s/\sigma_t)$.

TABLE I. Scattering target properties.

Scattering target	Molecule (or atom) equivalent	Maximum transmission in energy range used	Purity	Geometrical slant thickness (inches)	Physical form
Au	Au	0.03	99.9+% Au	1.41	Solid
Ni_2B[a]	$Ni_2B_{1.09}$	0.01	99.8% $Ni_2B_{1.09}$	1.4	Solid
B_2O_3	B_2O_3	0.11	99.9% B_2O_3	1.17	Solid
B^{10}	B^{10}	<0.005	94% B^{10} 4% B^{11} 2% Fe, Mg and Si	0.7	Powder

[a] The Ni_2B was prepared by Cooper Metallurgical Associates, Cleveland, Ohio, and hot pressed by the Norton Company, Niagara Falls, Ontario.

The B^{10} sample for transmission consisted of 0.698 g/cm² of the same powder used in the scattering measurements. Since thin samples of uniform density are difficult to prepare, it was decided to use a sample of fairly large geometrical thickness and to investigate it in the high energy region where its transmission could be measured easily.

The Ni_2B transmission sample was prepared using the powder from which the solid slab for the scattering measurements was made; and the same general considerations concerning thickness applied here. For the measurements of $(\sigma_t)_{Ni_2B}$, four independent sets of data were taken. The sample thickness was 3.90 g/cm².

For the B_2O_3 transmission measurements the sample

[29] Performed by Dr. John P. Nielsen, New York University.

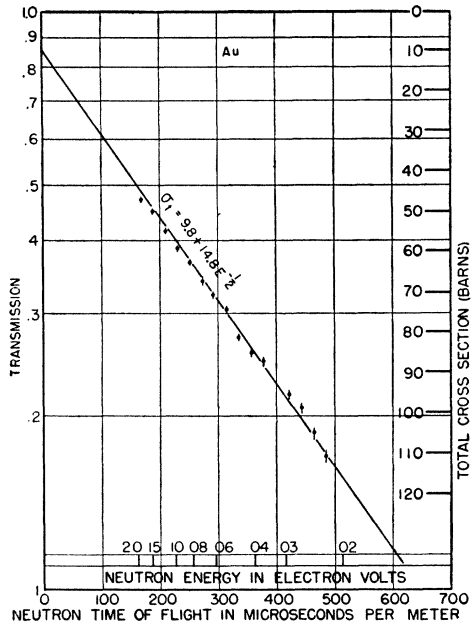

FIG. 5. Slow neutron transmission of 5.21 g/cm² of Au. The higher energy points fall below the linear $1/v$ curve as a result of the increasing importance of E relative to E_0 in the resonance denominator.

used was the solid slab used for the scattering investigations. The sample consisted of 4.03 g/cm².

In order to acquire as much data on the Au resonance as possible, using established techniques, the low energy region transmission for Au was investigated also. A 5.21 g/cm² sample was used in the region where

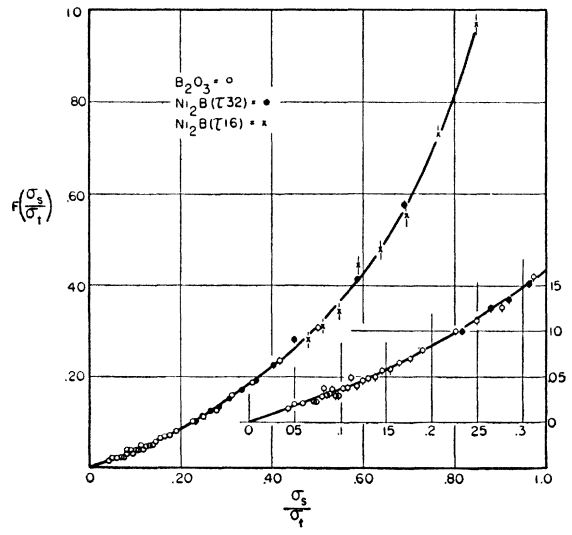

FIG. 6. The calibration function, $F(\sigma_s/\sigma_t)$. Open circles are points taken using B_2O_3 with arc-on (τ_a) and detection $(\tau_{dt})_e$ times of 32 microseconds; solid circles are points taken using Ni_2B with $\tau_a=\tau_{det}=32$ microseconds; crosses are points taken using Ni_2B with $\tau_a=\tau_{det}=16$ microseconds. Note excellent agreelment of Ni_2B and B_2O_3 data for $0.23<\sigma_s/\sigma_t<0.5$. Insert shows ower portion of curve on expanded scale.

$\Gamma^2 \ll 4(E-E_0)^2$. A least-squares fit of

$$\sigma_t=[\sigma_{c0}\Gamma^2(E_0/E)^{\frac{1}{2}}/4(E-E_0)^2]+\sigma_s(\text{const})$$

to the results of this measurement yielded

$\sigma_{c0}\Gamma^2=(638\pm16)$ b-ev², and $\sigma_s(\text{const})=(9.8\pm2)$ b.[30]

Here we have used $E_0=(4.87\pm0.07)$ ev, the most recent NVS value. These results are shown in Fig. 5. Since these Au measurements were taken at low neutron energy and transmission ~0.3, a $\frac{1}{3}$ standard filter[31] was used.

In addition, the transmission of 0.02745 g/cm² of Au was measured in the immediate vicinity of resonance. Since instrumental resolution does not allow the direct measurement of total cross section in this region, maximum information on the values of σ_{t0} and Γ can be obtained only by using the area[8] over the transmission dip, $\int_{-\infty}^{+\infty}[1-T(E)]dE$, neglecting σ_p and the $1/v$ dependence of σ_c. The area measured between 28.76- and 37.76-microseconds/meter neutron time of flight was (1.22±0.07) microseconds/meter.

Evaluation of the area integral by series expansion yields $A=(\Gamma/2)F(\alpha)$, where $F(\alpha)$ is a tabulated function and $\alpha=n\sigma_{t0}$, n being the number of Au atoms/cm² in the transmission sample. Correcting the value of the limited area to represent the area between the energy limits $-\infty$ and $+\infty$ allows direct comparison between measured and calculated areas.

VIII. TREATMENT OF DATA AND RESULTS

The measured calibration curve is shown in Fig. 6, where the points determined by Ni_2B and those determined by B_2O_3 are plotted together. The consistency between the two sets of measurements is readily apparent. If the scattering data for the B_2O_3 target were followed to higher energies (thus larger σ_s/σ_t values), we would expect the two sets of data to disagree somewhat, since the ratio of target thickness, a, to effective diffusion length for the two targets would be different. The fact that they do agree in the range of overlap, where they have small but somewhat different transmissions, substantiates the statement that the diffusion length criterion for thickness mentioned in Sec. III need not be invoked for $\sigma_s/\sigma_t<\sim0.5$ and $T<0.1$.

The rapid rise of $F(\sigma_s/\sigma_t)$ for large σ_s/σ_t and its approach to a value greater than unity for $\sigma_s/\sigma_t=1$ result from the following effect. For large values of σ_s/σ_t, multiple scattering becomes large, and this contributes to increased neutron density at greater depths in the scattering target. The subsequent "leakage" of neutrons out through the back of the target makes the total scattered neutron counting rate, which consists to a large extent of multiply scattered neutrons, dependent

[30] These results are essentially in agreement with earlier measurements by McDaniel, Sutton, Lavatelli, and Anderson, Phys. Rev. **72**, 729 (1947), who arrived at $\sigma_{c0}\Gamma^2=625$ b-ev², $\sigma_s(\text{const})=9.0$ b.

[31] Edward Melkonian, Phys. Rev. **76**, 1744 (1949).

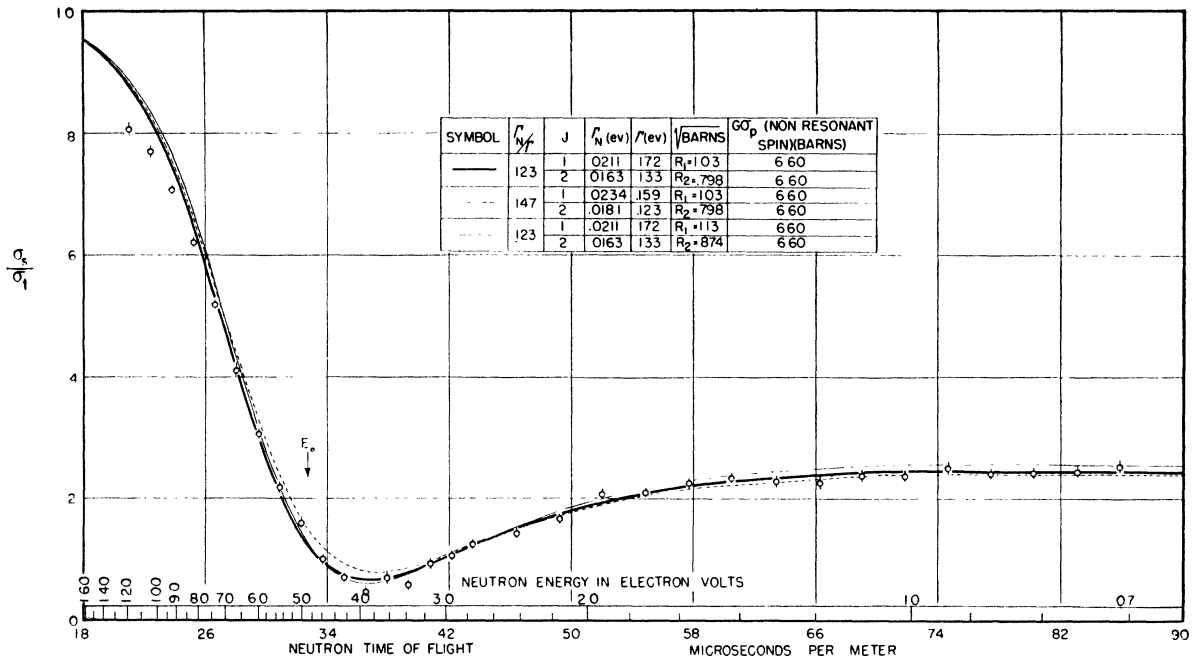

FIG. 7. The ratio $(\sigma_s/\sigma_t)_{Au}$ as a function of neutron time of flight. Heavy solid curve is best theoretical fit, calculated using Breit-Wigner one level formulas of Sec. I, with the level parameters indicated in the table. Effect of increasing Γ_N/Γ and $\sigma_{p\mp}$ by 20 percent are indicated by the dashed and thin solid curves, respectively. Discrepancy at large σ_s/σ_t values is explained by diffusion effect.

upon the ratio of target thickness to diffusion length. In effect, then, a larger fraction of the neutrons which would otherwise have been ultimately scattered to the counters "leaks" out the back of the C target than the Ni_2B target. Hence, the ratio $Nx_0/N_C=F(\sigma_s/\sigma_t)_{Ni_2B}$ approaches a value >1 as $(\sigma_s/\sigma_t)x_0\rightarrow 1$. For values of $\sigma_s/\sigma_t<\sim 0.5$, where only the singly, doubly, and triply scattered neutrons contribute appreciably to the total counting rate, the use of Eq. (1) is quite valid (see Appendix A).

This line of reasoning is borne out still further by noting that the "best fit" curve of Fig. 7 indicates that the measured values of $(\sigma_s/\sigma_t)_{Au}$ for $\sigma_s/\sigma_t>0.5$ are too small by a relative amount which increases with increasing σ_s/σ_t. This is due to the fact that for large σ_s/σ_t the ratio of slant thickness to diffusion length was not sufficiently great to use the infinite thickness approximation. As a result of this effect, the criterion that the experimental points for $(\sigma_s/\sigma_t)_{Au}<\sim 0.5$ be matched by a theoretical curve has been used in determining a best fit to the data.

Figure 7 contains the final experimental results in the form of $(\sigma_s/\sigma_t)_{Au}$ *vs* neutron time of flight. The method of determining the best group of parameters was as follows. Preliminary calculations of $\sigma_s(E)$, using very approximate values for the level parameters, indicated that σ_s has its minimum in the vicinity of 2 to 3 ev and that the dip is rather broad. At the minimum, $\sigma_s=G_{\pm}\sigma_{p\pm}$, the potential scattering contribution from the nonresonant spin state, and $(E_{min}-E_0)/(\Gamma/2)^2\gg 1$ so that σ_c is determined by $\sigma_{c0}\Gamma^2$, the value of which was already known. Thus, one of the scattering parameters was fixed. In the immediate vicinity of resonance, σ_s/σ_t is determined almost entirely by Γ_N/Γ, and somewhat farther away it is most sensitive to variations in $R_{\mp}$, the nuclear radius for the resonant spin condition. Successive approximations were made in Γ_N/Γ and $R_{\mp}$, using the relations

$$\Gamma^2=(\sigma_{c0}\Gamma^2/4\pi\lambda_0^2G_{\mp})/[(\Gamma_N/\Gamma)-(\Gamma_N/\Gamma)^2]$$

and $\sigma_{p\mp}=4\pi R_{\mp}^2$, choosing one of the possible values of $G_{\mp}$. Since $(\sigma_s/\sigma_t)_{Au}$ is insensitive to the value of Γ (except in the combination $\sigma_{c0}\Gamma^2$), the above procedure allows one to choose one value for $G_{\mp}$ and calculate σ_s/σ_t; to this same curve, however, there corresponds another set of values for Γ, Γ_N, and R. In this fashion it was found that the data are fit (heavy solid curve of

TABLE II. Measured and derived parameters for the 4.9-ev Au level.[a] (The correct choice of J is 1.)

E_0	4.87 ±0.07	
Γ_N/Γ	0.123±0.013	
$G_{\pm}\sigma_{p\pm}$	6.60±0.33	
J	1	2
$R_{\mp}$	1.03±0.09	0.798±0.06
Γ	0.172±0.01	0.133±0.009
Γ_N	0.0211±0.0018	0.0163±0.0015
$\sigma_{p\pm}$	10.6	17.6
$\sigma_{p\mp}$	13.3	8.0
σ_{to}	24,600	41,100

[a] Energies are measured in electron volts, cross sections in barns, and $R_{\mp}$ in barn$^{\frac{1}{2}}$; precisions are estimated; and E_0 is the most recent NVS value of Rainwater and Havens.

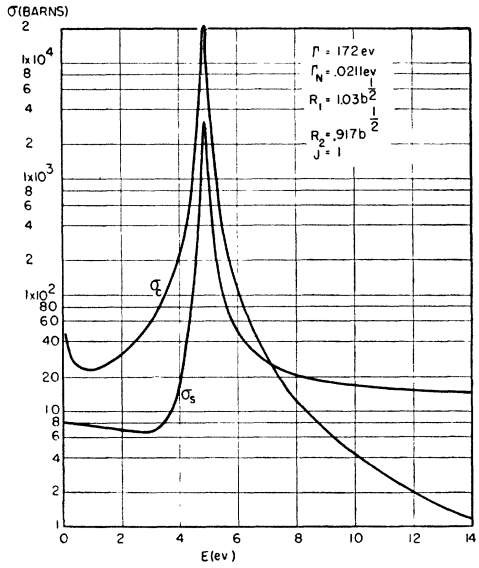

FIG. 8. Theoretical curves of $\sigma_c(E)$ and $\sigma_s(E)$ for Au, calculated using best fit parameters indicated, assuming $J=1$ for the 4.87-ev level.

Fig. 7) by using

$$4\pi\lambda_0^2(G\Gamma_N^2)=89.3 \text{ b-ev}^2,$$
$$16\pi\lambda_0(G\Gamma_N R)=84.5 \text{ b-ev}^2,$$
$$\sigma_p(\text{total})=11.6 \text{ b}.$$

The level parameters corresponding to each of the two possible values of J are presented with estimates of precision in Table II.

To indicate the sensitivity of various parts of the theoretical form of σ_s/σ_t *vs* E, we have, in Fig. 7, presented the curves calculated for Γ_N/Γ larger than optimum by 20 percent and for $\sigma_{p\mp}$ larger than optimum by 20 percent. In Fig. 8 are shown the theoretical curves for $(\sigma_c)_{\text{Au}}$ and $(\sigma_s)_{\text{Au}}$, individually, calculated using the parameters indicated by the choice $J=1$.

In an attempt to decide upon the value of J, the following information may be considered.

A. The experimental value of $\int_{-\infty}^{+\infty}[1-T(E)]dE$, discussed in Sec. VII, is (0.382 ± 0.027) ev. The calculated area, using the parameters of Table II for $J=1$, is 0.372 ev, and the area calculated for $J=2$ is 0.404 ev. Although the experimental area agrees better with the choice $J=1$, the possibility that $J=2$ cannot be ruled out because of the 7 percent uncertainty in the experimental area.

B. Since $G_{\pm}\sigma_{p\pm}$ is found to be 6.60 b, and two distinct possible values for R are indicated, $\sigma_{p\pm}$ and $\sigma_{p\mp}$ are determined for each possible value of J.

As indicated in Table II, the partial potential scattering cross section, $\sigma_{p\pm}$, takes the values of 10.6 b and 17.6 b for $J=1$ and $J=2$, respectively. Since this cross section is far from a resonance with the spin state in question, it is to be expected that it will take a value fairly close to the geometric cross section of Au, i.e., approximately $4\pi(0.15A^{\frac{1}{3}})^2=9.6$ b. These considerations are in favor of the choice $J=1$. The values $\sigma_{p\mp}=13.3$ b or 8.0 b fall on opposite sides of 9.6, but neither is very far away from the values 9.0 and 11.0 for Bi and Pb, for example. The precision is somewhat poorer for $\sigma_{p\mp}$ than for $\sigma_{p\pm}$, so we may conclude that $\sigma_{p\pm}$ strongly favors $J=1$, while $\sigma_{p\mp}$ does not contradict this result.

C. The activation[32] measurement of Coster *et al.*,[33] as corrected by Groendijk,[34] yields $\sigma_{c0}\Gamma=4290$ b-ev. The present authors estimate accuracy limits of $\sim\pm30$ percent on this figure. The two values calculated from the results of the present experiment are: $J=1$, $\sigma_{c0}\Gamma=3690$ b-ev; $J=2$, $\sigma_{c0}\Gamma=4800$ b-ev. Certainly, no positive conclusion can be drawn from this datum. However, it is not inconsistent with $J=1$.

D. A fourth criterion which might be used to determine the value of J is the comparison of the measured value for the resonance scattering integral[22] in a $1/E$ flux, $\sum_s$, with the two values calculated using our results. Using the data of Table II we get: $J=1$, $\sum_s=168$ b; $J=2$, $\sum_s=218$ b. Harris, Muehlhause, and Thomas[22] give the experimental value $\sum_s\sim210$ b. This is the only evidence we have found which might be construed to contradict the choice $J=1$. However, Muehlhause[35] states that this value is expected to be too large, perhaps by as much as ~50 percent, since it includes the effects due to higher levels with large scattering. From these considerations we conclude that this evidence leans in favor of $J=1$, although $J=2$ is not definitely ruled out.

E. The possible values of $(\sigma_{t0})_{\text{Au}}$ calculated from the results of the present experiment, listed in Table II, are: $J=1$, $\sigma_{t0}=24{,}600$ b; $J=2$, $\sigma_{t0}=41{,}100$ b. Since these two values are quite different, it would seem that even a relatively rough experimental determination of σ_{c0} (or σ_{t0}) should strongly indicate the choice of J. By measurement of the cross section for self-indication,[36] neglecting resonance scattering effects, Frisch[37] gives the value $\sigma_0=26{,}000$ b. Although the agreement with $J=1$ seems quite good, this may be somewhat fortuitous in view of the large errors which were later found to be associated with early self-indication experiments. However, a more recent self-indication experiment by Goldhaber,[38] using several thicknesses of Au, yielded the value $\sigma_0=25{,}000$ b with a maximum uncertainty of ±5000 b.

In view of the affirmative data presented in A, B, D, and particularly E, and the lack of contradiction in C, one can conclude that $J=1$ for the resonance level.

[32] Reference 2, pp. 141–143.
[33] Coster, De Vries, and Diemer, Physica **10**, 281 (1943).
[34] H. Groendijk, thesis, Groningen (1949).
[35] C. O. Muehlhause, private communication.
[36] Reference 2, pp. 140, 141, 147, 148.
[37] O. Frisch, K. Danske Vidensk. Selsk. **14**, No. 12 (1937).
[38] M. Goldhaber (private communication). This measurement does not include a correction for scattering, nor for Doppler effect. Neither correction, however, would be large enough to invalidate the conclusion drawn.

The value of $\Gamma_N/\Gamma=\sum_s/(\sum_s+\sum_a)=0.14$ (to be compared with the result of the present experiment, $\Gamma_N/\Gamma=0.123$) has been calculated by Harris *et al.*[22] on the basis of their measurement of $\sum_s$ and a calculated value for $\sum_a$, the resonance capture integral in a $1/E$ flux. The value they used for $\sum_a$, 1296 b, however, is based upon earlier Columbia NVS measurements and is somewhat in error according to calculations based on the results of Table II. Thus, even if their measured value of $\sum_s$ agreed with that calculated from the present measurements, one would expect some disagreement in Γ_N/Γ. We get for $J=1$, $\sum_a=1180$ b. Furthermore, their measured value $\sum_s\sim 210$ b includes the effects of higher levels, as mentioned previously. In view of these considerations and the large probable error allowed their measurements, their result is essentially in agreement with ours.

Our total potential scattering cross section, $(G_\pm\sigma_{p\pm}+G_\mp\sigma_{p\mp})$, is (11.6 ± 1) b. Hibdon and Muehlhause,[18] using Co and Mn scattering detectors, measured the values 10.6 and 10.8 b. It is to be noted, however, that their values reflect conditions at considerably higher energies than those used in our measurements. If the energies at which their measurements were taken are far from resonances, however, we should compare their results with our measured value of $\sigma_{p\pm}$ and not with $(G_\pm\sigma_{p\pm}+G_\mp\sigma_{p\mp})$ (see B above). In that case, for the choice $J=1$, our value of $\sigma_{p\pm}=10.6$ b is in excellent agreement with theirs.

Figure 9 shows the results of high energy scattering from the Au target. The target, in this energy region, is not in general thick in the sense of Sec. III, and since σ_s/σ_t is large, it was felt that the conversion of the data into σ_s/σ_t values according to the calibration curve would be misleading. Hence, N_{Au}/N_C is plotted *vs* time of flight. The dips in the vicinity of 75 ev and between 300 to 500 ev represent, effectively, rises in the percentage of capture present, i.e., the presence of resonances. Since the resolution is quite poor, no analysis can be made. However, in view of the magnitude of the effect and the relatively broad resolution used, we can assert that in both cases capture plays an appreciable role. The dip at $\sim$75 ev may be the result of one or more resonances, while that at 300 to 500 ev is almost certainly the smeared out effect of a number of levels. This latter is, no doubt, the same group of levels noted by Hibdon and Muehlhause.[18]

The authors wish to express their appreciation to Professors L. J. Rainwater and W. W. Havens, Jr., for their active guidance and invaluable suggestions, and to Dean J. R. Dunning for his constant encouragement and advice during the course of the work.

Thanks also are due the United States Atomic Energy Commission for their support of this research.

APPENDIX A. MULTIPLE SCATTERING ANALYSIS

Consider the single scattering event illustrated in Fig. 2. If n is the number of scattering nuclei per unit volume, $N_0(E)$ the incident flux density, and $\alpha S(E)$ the counter detection sensitivity for neutrons emitted isotropically from the element dz, where $S(E)$ indicates the $1/v$ dependence of the BF_3 counter sensitivity and α is a geometrical factor depending on the position of the element in question, then the number of neutrons singly scattered from the lamina dz is

$$dN_1=\alpha S(E)[N_0(E)\exp(-n\sigma_t z)][n\sigma_s dz]\times[\exp(-n\sigma_t z\cos\theta_0/\cos\theta_1)]. \quad \text{(A-1)}$$

Integrating (A-1) from $z=0$ to $z=a$ gives the number of neutrons counted, arising due to single scattering into unit solid angle about θ_1 from the cylindrical element indicated. It is found

$$N_1=\alpha S(E)N_0(E)(\sigma_s/\sigma_t)\left[\frac{1}{1+(\cos\theta_0/\cos\theta_1)}\right]\times[1-T^{[1+(\cos\theta_0/\cos\theta_1)]}], \quad \text{(A-2)}$$

where we set $T=\exp(-n\sigma_t a)$ as the target transmission. Noting that $\langle\cos\theta_0/\cos\theta_1\rangle_{Av}\approx 1$, we see that the last factor is approximately T^2 and that if $T<0.1$, an error of $<\sim$1 percent is made in N_1 by neglecting the term in T. Calling the remaining geometrical factor $f_1(\theta_0,\theta_1)$ we can write

$$N_1=\alpha S(E)N_0(E)f_1(\theta_0,\theta_1)(\sigma_s/\sigma_t). \quad \text{(A-3)}$$

Iteration of the above procedure, using the element dz as a source point and neglecting edge effects, then yields similar expressions for successive multiplicities of scattering. Thus, the total counting rate due to neutrons originally scattered in the cylindrical element shown and leaving the target x in the direction θ_1 becomes

$$N_x=\alpha S(E)N_0(E)\sum_{j=1}^{\infty} f_j(\theta_0,\theta_1)(\sigma_s/\sigma_t)_x{}^j. \quad \text{(A-4)}$$

It is assumed that T and σ_s/σ_t are sufficiently small so that negligible diffusion out the back of the target occurs. Division of (A-4) by the similar expression for a carbon target, in which energy dependence arises only through the factors $S(E)$ and $N_0(E)$, then yields

$$N_x/N_C=\sum_{j=1}^{\infty} g_j(\sigma_s/\sigma_t)_x{}^j, \quad \text{(A-5)}$$

which obviously applies for the total counting rate ratio, where the g_j are factors depending on geometry alone. We define the ratio N_x/N_C as $F(\sigma_s/\sigma_t)_x$, the scattering ratio to carbon, for infinitely heavy nuclei. A fit of (A-5) to the curve of Fig. 6 indicates that only the first three terms contribute appreciably for $(\sigma_s/\sigma_t)<\sim$0.5.

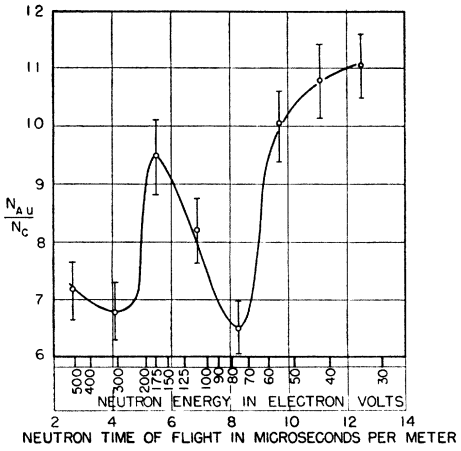

FIG. 9. Ratio of thick target neutron scattering from Au to that from moderately thick graphite. Dips at $\sim$80 ev and $>$300 ev indicate the presence of levels with appreciable capture.

APPENDIX B. BACKGROUND AND ENERGY LOSS CORRECTIONS

The quantities N_x and N_C in (A-5) represent counting rates *due to scattering* from targets x and C. Then if B represents counting rate due to background when a thick target is in position, $N_x = N_x' - B$, where N_x' is the measured counting rate when x is the scatterer. Letting primes indicate *measured* counting rates generally, we also have $N_{B^{10}} = N_{B^{10}}' - B$ and the left-hand side of (A-5) can be written as

$$\frac{N_x}{N_C} = \frac{N_x' - B}{N_C' - B} = \frac{N_x' - N_{B^{10}}'}{N_C' - N_{B^{10}}'} + \frac{N_{B^{10}}}{N_C' - N_{B^{10}}'}, \tag{A-6}$$

where we have neglected $N_{B^{10}}$ in the denominator since $N_{B^{10}} \ll (N_C' - N_{B^{10}}')$. Since the second term on the right-hand side of (A-6) is small for $x = Ni_2B$ or B_2O_3, we can combine (A-5) and (A-6) to give

$$F(\sigma_s/\sigma_t)_{x_0} = \frac{N_{x_0}' - N_{B^{10}}'}{N_C' - N_{B^{10}}'}\left[1 + \frac{(\sigma_s/\sigma_t)_{B^{10}}}{(\sigma_s/\sigma_t)_{x_0}}\right]. \tag{A-7}$$

The bracketed factor then corrects the background measurement for the small B^{10} scattering contribution. A similar analysis yields for Au

$$F(\sigma_s/\sigma_t)_{Au} = \frac{N_{Au}' - N_{B^{10}}'}{N_C' - N_{B^{10}}'} + F(\sigma_s/\sigma_t)_{B^{10}}. \tag{A-8}$$

Since $F(\sigma_s/\sigma_t)$ has been defined as the scattering ratio to carbon for infinitely heavy nuclei, the right-hand sides of (A-7) and (A-8) must further be multiplied by the factors indicated in Secs. III B and III C to correct at least the "singly scattered" counting rate for the finite mass effect. The latter correction arises in the following manner. In writing (A-1) above, the σ_t appearing in the last bracket is more correctly σ_t', the cross section of the target nuclei for neutrons of energy $E' < E$ after collision. Then using the fact that $\langle \cos\theta_0/\cos\theta_1 \rangle_{Av} \approx 1$, (σ_s/σ_t) in (A-2) becomes $2\sigma_s/(\sigma_t + \sigma_t')$. Thus, multiplication of the right-hand sides of (A-7) and (A-8) by $(\sigma_t + \sigma_t')/2\sigma_t$ corrects for this effect.

PHYSICAL REVIEW VOLUME 83, NUMBER 4 AUGUST 15, 1951

Configuration Interaction in Mn II

R. E. TREES
University of Pennsylvania, Philadelphia, Pennsylvania
(Received May 2, 1951)

The theoretical formulas for d^6 and d^5s are compared with the experimental data of Mn II. The relative positions of these configurations in Mn II allow the magnitude of configuration interaction to be determined accurately without the use of a least-squares calculation. Over-all agreement between theory and experiment is improved by the use of separate parameters in the two configurations and by the introduction of the effects of configuration interaction.

The positions of the terms not yet known experimentally are predicted as a help in further analysis of this spectrum. The positions of terms of the d^5s configuration are believed to be predicted with better than usual accuracy by the use of a correction term proportional to $L(L+1)$.

I. TERM VALUES OF Mn II WITHOUT CONFIGURATION INTERACTION

CURTIS[1] has recently extended the experimental analysis[2] of the $3d^54s$ and $3d^6$ configurations of Mn II to include some of the triplet terms, thus making possible a further theoretical analysis of this spectrum.

The term values in Russell-Saunders coupling for the d^5s configuration of Mn II have been calculated by Bowman[3] without allowance for configuration interaction; his results are valid for the terms which are only slightly affected by configuration interaction (i.e., the majority of terms in d^5s), since his least square fit was based on terms that are probably almost free of effects of configuration interaction. We have repeated his least-squares calculation, but have included the additional experimental values[1] for d^5s. The results are given in part (1) of Table I and are essentially in agreement with Bowman's results (the mean deviation of his data is 447 cm^{-1} compared to 412 cm^{-1} for the d^5s terms in Table I). A comparison of the d^6 data with theory, also neglecting effects of configuration interaction, is given in the same column. The mean deviation between theory and experiment, using separate parameters in d^5s and d^6 and neglecting configuration interaction is 678 cm^{-1}.

The parameters used in the calculation of Table I are those in the formulas of Racah.[4] The d^6 formulas are in the same form as the d^4 formulas with "$6A$" replaced by "A." In the d^5s formulas, "$10A$" (in Racah's formulas for d^5) was replaced by "D" and the proper multiple of G_2 was subtracted.[5] The parameters were evaluated by least squares.

An effort was made to fit the data using the same B and C parameters in d^5s and d^6, again neglecting configuration interaction, with the result shown in part 2

[1] C. W. Curtis, Phys. Rev. **78**, 343 (1950).
[2] Other experimental values were taken from C. W. Curtis, Phys. Rev. **53**, 474 (1938). The ^5D of $3d^6$ and the ^7S and ^5S of $3d^54s$ were found previously by M. A. Catalan, Phil. Trans. Roy. Soc. (London), **A223**, 127 (1922); An. Soc. Espan. **26**, 67 (1928); Russell, Astrophys. J. **66**, 233 (1927); and Black and Duffendack, Science **66**, 402 (1927).
[3] D. S. Bowman, Phys. Rev. **59**, 386 (1941). The term values for d^5 configuration were first calculated by M. A. Catalan and M. T. Antunes, Z. Physik **102**, 432 (1936).
[4] G. Racah, Phys. Rev. **62**, 438 (1942); **63**, 367 (1943). These are referred to as II and III, respectively.
[5] J. H. Van Vleck, Phys. Rev. **45**, 405 (1934).